Biomaterials Science

Accepted Manuscript

This article can be cited before page numbers have been issued, to do this please use: Y. Wang, K. Kostka-Wirtz, N. Bartelsen, K. Loza, C. Weingärtner, P. Arnold, D. Damm, K. Überla, M. Epple and V. Temchura, *Biomater. Sci.*, 2026, DOI: 10.1039/D5BM01792K.

ROYAL SOCIETY OF CHEMISTRY

rsc.li/biomaterials-science

View Article Online
DOI: 10.1039/D5BM01792K

Silica-coated papillomavirus-based nanoparticles: a shielded scaffold for HIV-1 vaccines.

Yu Wang[1,*], Kathrin Kostka-Wirtz[2,*], Nils Bartelsen[1], Kateryna Loza[2], Christoph Weingärtner[1], Philipp Arnold[3], Dominik Damm[1], Klaus Überla[1], Matthias Epple[2,**], Vladimir Temchura[1,**]

[1] Harald zur Hausen Institute of Virology, Universitätsklinikum Erlangen, Friedrich-Alexander-Universität Erlangen-Nürnberg (FAU), 91054 Erlangen, Germany

[2] Inorganic Chemistry and Center for Nanointegration Duisburg-Essen (CENIDE), University of Duisburg-Essen, 45141 Essen, Germany

[3] Institute of Functional and Clinical Anatomy, Friedrich-Alexander-Universität Erlangen-Nürnberg (FAU), 91054 Erlangen, Germany

* equal contribution
** equal contribution

Corresponding author:
Prof. Dr. Vladimir Temchura
Harald zur Hausen Institute of Virology,
Universitätsklinikum Erlangen
Schlossgarten 4
91054 Erlangen
Germany
E-Mail: vladimir.temchura@fau.de
Tel: +49-9131-85-43652
Fax: +49-9131 85-32101

Abstract

View Article Online
DOI: 10.1039/D5BM01792K

The development of a safe, effective, and accessible human immunodeficiency virus 1 (HIV-1) vaccine remains a global priority, and nanoparticles (NPs) have emerged as a promising platform for vaccine delivery. However, the efficacy of protein-based NP vaccines is often limited by pre-existing immunity against scaffold components. In this study, we developed a novel HIV-1 vaccine platform by converting self-assembling human papillomavirus (HPV) L1 virus-like particles (VLPs) into immune-stealth biomaterials for focused antigen delivery. Encapsulation of VLPs within a silica shell provided both immune shielding and a surface for site-specific antigen conjugation. The resulting L1-SiO_2 NPs were covalently functionalized with HIV-1 Env trimers (L1-SiO_2-Env) and characterized for their physicochemical properties and immunogenicity. In vivo, the silica coating effectively masked L1-specific B cell epitopes, reduced anti-scaffold IgG responses and enhanced Env-specific antibody production in mice pre-immunized against HPV. This synthetic strategy offers a versatile platform for overcoming scaffold-directed immunity in nanoparticle vaccines.

Keywords: Silica-coated nanoparticles, HPV L1 virus-like particles, HIV-1 Env vaccine delivery, immune shielding

1. Introduction

View Article Online
DOI: 10.1039/D5BM01792K

The global burden of HIV underscores the urgent need for a safe, effective, and accessible preventive vaccine. Despite more than four decades of research, no licensed HIV vaccine has been approved. This persistent challenge is largely due to high variability and sophisticated immune evasion strategies of the virus, alongside suboptimal vaccine delivery systems [1-3]. Ideal vaccine candidates must induce robust, durable, and focused immune responses while being safe and scalable [4, 5].

Nanoparticles (NPs) have emerged as powerful tools for enhancing subunit vaccine efficacy. Their size, multivalency, and capacity for targeted delivery enable improved antigen uptake, B cell activation, and lymph node trafficking [6-9]. Displaying viral antigens on NP scaffolds at high density can overcome immune tolerance and stimulate otherwise weakly responsive B cell populations [10]. Among NP systems, self-assembling virus-like particles (VLPs) with conjugated antigens have been introduced as effective biomolecular scaffolds of biological origin for enhancing both the magnitude and quality of antibody responses through multivalent presentation of displayed antigens [11, 12]. Consequently, VLPs are widely used in next-generation vaccine design due to their versatility, safety profiles, and significant efficacy in clinical trials [13]. However, a pre-existing immunity against scaffold proteins may attenuate immune responses to the conjugated antigens, thereby reducing the overall effectiveness of the vaccine formulation [14]. Overcoming such anti-scaffold immunity still remains a key challenge for nanoparticle vaccine design.

In our previous work, we demonstrated that self-assembling human papillomavirus (HPV) L1 protein VLPs can be functionalized with viral glycoprotein antigens, establishing them as highly immunogenic and structurally stable NP scaffolds for vaccine development [15]. Yet, widespread HPV vaccination has led to population-wide anti-L1 immunity, which may compromise the effectiveness of L1-based vaccines by accelerating particle clearance and diverting immune responses.

In this study, we introduce a materials-engineering strategy to address this challenge by coating HPV-16 L1 VLPs with a silica shell. The silica layer acts both as an immune-

View Article Online
DOI: 10.1039/D5BM01792K

shielding and a surface-functionalization interface, preserving the structural integrity of the protein scaffold while providing reactive silanol groups for covalent conjugation of HIV-1 envelope (Env) trimers. We systematically studied the physicochemical properties, the B cell activation potential, and the immunogenicity of these silica-coated VLPs. Furthermore, we demonstrate that this hybrid inorganic–organic design enables a targeted antigen delivery with minimized scaffold-directed immunity. Thus, we show that the silica coating of VLPs is an applicable method for nanoparticle vaccine development.

2. Methods

2.1 Preparation of L1-VLP scaffold

Self-assembled HPV-16 L1-VLPs were produced from *E. coli*, following a previously described protocol [15]. Briefly, the coding sequence for the HPV-16 L1 protein, lacking the twenty-nine N-terminal amino acids, was cloned into the pET-100 expression vector (Thermo Fisher, Waltham, MA, USA) and transformed into BL21 (DE3) competent cells (Thermo Fisher, Waltham, MA, USA). L1 protein expression was induced with 0.5 mM isopropyl β-D-1-thiogalactopyranoside (IPTG; Thermo Fisher, Waltham, MA, USA). The bacterial cells were lysed by sonication (Branson Ultrasonics S-450A, USA) to release the soluble L1 proteins. High-purity L1 proteins were obtained through a three-step purification process involving ammonium sulfate precipitation (Carl Roth, Karlsruhe, Germany), ion-exchange chromatography, and size-exclusion chromatography (both from Cytiva, Marlborough, MA, USA). At this stage, 20 mM dithiothreitol (DTT; Thermo Fisher, Waltham, MA, USA) was added to the buffer to obtain L1 pentamers. The pentamers were self-assembled into VLPs *in vitro* by dialysis (SnakeSkin Dialysis Tubing, 10K MWCO, Thermo Fisher, USA), which removed DTT and reduced the pH from 7.5 to 6.0.

2.2 Wrapping L1-VLP with a silica shell and functionalized with azide groups

The L1-VLPs were first concentrated to 1 mg/mL by spin filtration. In the next step, 500 µL of the aqueous L1-VLP dispersion was mixed with 850 µL aqueous polyethyleneimine (PEI, Linear, 25K, Surflay Nanotec GmbH, Berlin, Germany) solution (2 mg/mL) or aqueous PEI-

View Article Online
DOI: 10.1039/D5BM01792K

Cy5 (Surflay Nanotec GmbH, Berlin, Germany) solution (2 mg/mL), respectively, and stirred for 10 min. Then, a mixture of 4.5 mL ethanol (VWR International GmbH, Darmstadt, Germany), 11.4 µL 7.8% ammonia solution (Carl Roth, Karlsruhe, Germany) and 5.7 µL tetraethylorthosilicate (TEOS, Sigma-Aldrich, Merck, Germany) was added to the PEI- or PEI-Cy5-stabilized VLPs, respectively. The dispersion was stirred for 16 h under light exclusion. The L1-VLPs were isolated by centrifugation for 30 min and 14,200 rpm by spin filtration. The particles were redispersed with ultrasonication for 6 s in 500 µL water.

The L1-SiO_2 particles were surface-functionalized with azide groups (L1-SiO_2-N_3) by adding 500 µL of the L1- SiO_2 dispersion to a solution of 2 mL ethanol, 7.6 µL (3-azidopropyl)triethoxysilane (SelectLab Chemicals GmbH, Münster, Germany), and 2.6 µL ammonia solution (7.8%) and stirring for 6 h under light exclusion at room temperature. The resulting dispersion was centrifuged for 30 min at 14,200 rpm by spin filtration and, after subsequent addition of 500 µL ultrapure water, redispersed for 8 s with a sonotrode.

2.3 Preparation of L1-SiO_2-Env or L1-Env

HIV-1 Env trimers were covalently linked to the nanoparticles via orthogonal conjugation, utilizing C-terminal aldehyde-tagged (LCTPSR) HIV-1 Env trimers (Env-Ald_6) [16]. In short, we used cleavage-independent, soluble BG505 trimers with the gp120 subunit and the gp41 ectodomain covalently connected via a flexible 2x G_4S linker originally described by Prof. Dr. Rich Wyatt [17]. These trimers were engineered to mimic the native-like pre-fusion conformation of Env, which displays multiple epitopes for broadly neutralizing antibodies. In a previous study, we introduced a genetically encoded aldehyde-tag (LCTPSR) at the C-termini of the trimers. The cysteine in this motif gets converted by endogenous formylglycine-generating enzyme (FGE). The resulting formylglycine bears an unique aldehyde group in the side chain enabling chemical targeting by aminooxy groups [16]. Env proteins and FGE were transiently co-expressed in 293F suspension cells (Thermo Fisher, Waltham, MA, USA) to promote aldehyde group formation. The Env-Ald_6 trimers were purified from the culture supernatant using lectin affinity chromatography with agarose-bound *Galanthus nivalis* lectin (Vector Laboratories Inc., Burlingame, CA, USA). The purified Env-Ald_6 was then incubated overnight at 37°C with the linker DBCO-PEG_3-

View Article Online
DOI: 10.1039/D5BM01792K

oxyamine (Broadpharm, San Diego, CA, USA) under oxime reaction conditions (250 mM NaAC, pH 4.5) at 400 rpm, producing DBCO-terminated Env-Ald_6 (Env-DBCO). After buffer exchange via ultrafiltration (Amicon® Ultra-15, 100 kDa MWCO, Merck, Germany), Env-DBCO was conjugated to L1-SiO_2-N_3 or to azide-PEG_4-NHS (Merck, Germany) pre-treated L1-VLP (L1-N_3) via a non-catalyzed click reaction (4°C, 18 h), purified by centrifugation (3 times in PBS, 30min at 12,000 rpm in 4°C) and yielded L1-SiO_2-Env or L1-Env NPs. Previously, we confirmed via conformational ELISA and FACS that both the oxime reaction conditions (no salt, low pH) and the coupling procedure do not result in a significant reduction of Env pre-fusion conformation [16].

2.4 NP analysis

Transmission-Electron Microscopy (TEM) of particles was performed as described before [15, 18]. Particles were diluted in PBS and then washed with 2% uranyl acetate twice after application to a freshly glow-discharged carbon covered cupper grid (Science Service Munich, Germany). After air drying, samples were imaged in a JEOL1400Plus TEM (JEOL, Garching, Germany) operating at 120 kV. Scanning transmission electron microscopy (STEM) in scanning electron microscopy mode (STEM-in-SEM) was carried out with an Apreo S LoVac system (Thermo Fisher Scientific, USA). L1-VLP and L1-SiO_2 NP dispersions were applied to copper grids coated with an ultrathin amorphous carbon film and subsequently air-dried. The prepared grids were then allowed to dry in air at room temperature. Energy-dispersive X-ray spectroscopy (EDX) mappings were performed with an Apreo S LoVac microscope (ThermoFisher Scientific Inc., USA). Dynamic light scattering (DLS) and zeta potential measurements were carried out with a Zetasizer Nano ZS (λ = 633 nm, Malvern Nano ZS ZEN 3600, UK). UV–Vis spectroscopy was performed with a Varian Cary 300 Bio spectrophotometer (Agilent Technologies, USA) in 400 µL Suprasil® quartz cuvettes.

Fluorescence imaging was performed with a Keyence Biorevo BZ-9000 fluorescence microscope (Germany) with a TRITC filter (Ex. 540 ± 25 nm, DM 565 nm, BA 605 ± 55 nm) and a GFP-B filter (Ex. 470 ± 40 nm, DM 495 nm, BA 535 ± 50 nm). Additionally, a Leica TCS SP8X FALCON confocal laser scanning microscope (CLSM; Leica, Germany) was

used, equipped with laser wavelengths of 405 nm, 488 nm, and 647 nm, a pulsed laser WLL (470–670 nm), and an HC PL APO UVIS CS2 63X/1.2 water immersion lens.

View Article Online
DOI: 10.1039/D5BM01792K

2.5 Mice

The study involved two types of mice: female wild-type (WT) mice and PGT121 mice. The WT mice were of the C57BL/6NRj strain, sourced from Janvier Labs in France. The PGT121 mice, an in-house bred strain, were specific for the HIV-1 Env protein and carried a B cell receptor transgene. These mice were provided by Dr. Michel Nussenzweig from Rockefeller University in New York, USA. For this study, only female WT mice were used, whereas both male and female PGT121 mice were included to ensure a diverse representation of the transgenic strain. All mice were accommodated in ventilated cages at the animal facility (Franz-Penzoldt-Center) of the Faculty of Medicine, FAU (Erlangen, Germany) and handled as recommended by the Federation of European Laboratory Animal Science Association and as approved by the Government of Lower Franconia (license 55.2.2-2532-2-1199). Mice were euthanized after experiments or for organ donations by CO_2 treatment with subsequent cervical dislocation.

2.6 B cell activation *in vitro*

WT and PGT121 B cells were isolated using a MACS-based isolation kit specifically designed for murine naive B cells, in accordance with the manufacturer's protocol (Miltenyi Biotec, Bergisch-Gladbach, Germany). A total of 2 x 10^5 cells were subsequently plated into U-bottom 96-well cell culture plates (Greiner Bio-One, Germany), with 100 µL of R10 medium per well. The medium consisted of RPMI 1640 (Thermo Fisher, USA) supplemented with 10% fetal calf serum (FCS, Capricorn Scientific GmbH, Ebsdorfergrund, Germany), 1% penicillin-streptomycin (Sigma-Aldrich, Merck, Germany), 10 mM 4-(2-hydroxyethyl)-1-piperazineethanesulfonic acid (HEPES, Thermo Fisher, USA), 2 mM L-glutamine (Thermo Fisher, USA), and 50 µM 2-mercaptoethanol (Thermo Fisher, USA). Once the cells were seeded, nanoparticle dilutions were prepared in 100 µL of R10 medium and added to each well, resulting in a final volume of 200 µL per well. The plates were then incubated at 37°C with 5% CO_2 for 24 hours to allow interactions between the NPs and the

B cells. Lipopolysaccharide (LPS; Merck, Germany), a polyclonal B cell activator, was used as a positive control. Following incubation, cells were stained with anti-CD19-Qdot655, anti-CD86-FITC, anti-CD40-PE and the fixable viability dye eFluor450 (Thermo Fisher Scientific, Waltham, MA, USA). The activation status of live B cells was assessed using a spectral flow cytometer (Cytek Northern Lights, USA) and data analysis was performed with FlowJo software (BD Biosciences, USA).

2.7 Immunization

Vaccine candidates were administered intramuscularly (i.m.) into the hind legs of each mouse under isoflurane anesthesia (CP-Pharma, Burgdorf, Germany). A total of 60 µL per mouse was injected, evenly distributed between both hind legs. Blood samples were collected from the retrobulbar venous plexus. Minicaps® (Hirschmann, Eberstadt, Germany) were used for blood collection, and samples were placed in BD Microtainer® tubes (Becton Dickinson, Franklin Lakes, NJ, USA). The samples were centrifuged at 5000 rpm for 5 min to separate the serum. Env-specific and L1-specific antibody levels in the serum were then analyzed using ELISA, following previously established protocols.

2.8 Analysis of humoral immune responses

To assess Env- or HPV-specific antibody levels in vaccinated mouse sera, 150 ng of BG505 Env protein or 500 ng of L1 protein were diluted in 100 µl ELISA coating buffer per well and incubated overnight at 4 °C in white, high-binding, flat-bottomed 96-well assay plates (Greiner, Kremsmünster, Austria). Following overnight incubation, wells were blocked using 5% skimmed milk in PBS/T (PBS containing 0.05 % of Tween-20). Serum samples diluted at 1:1250 in PBS/T were then added to the wells. After three washes, HRP-conjugated anti-mouse IgG (Dianova, Hamburg, Germany), at a 1:5000 dilution in PBS/T was added and incubated for 60 min at room temperature (RT). Plates were washed again before addition of 70 µL of ECL solution (0.1 M Tris, 250 mg/L luminal sodium salt, 22 mg/L p-coumaric acid, 3.4 µL 30% H_2O_2 ad 10 mL H_2O) per well, and luminescence was measured with a Victor X4 multi-label plate reader (PerkinElmer, Waltham, MA, USA).

2.9 Statistical analysis

View Article Online
DOI: 10.1039/D5BM01792K

All experimental data were analyzed using GraphPad Prism software. Statistical significance between groups (Figure 5 and 9) was determined by one-way ANOVA followed by Tukey's post hoc test for multiple comparisons. For Figure 10 statistical analysis was assessed using two-tailed unpaired t-test. A p-value of less than 0.05 was considered statistically significant.

3. Results

3.1 Synthesis and Characterization of L1-SiO_2 NPs

Recombinant self-assembled L1-VLPs were produced from soluble HPV16 L1 proteins derived from *E. coli* following a previously described protocol [15]. The morphology of the purified L1-VLPs was confirmed by TEM (**Figure 1A**). Size analysis of 50 particles from STEM images (**Figure 1B**) using ImageJ software revealed an average diameter of 53 ± 7 nm. The hydrodynamic diameter and zeta potential of the L1-VLPs were subsequently determined by dynamic light scattering (DLS) (**Table 1**).

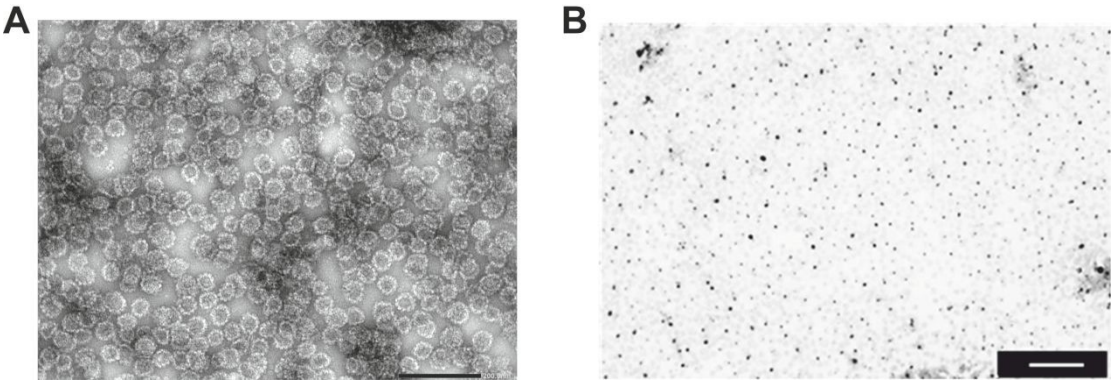

Figure 1. Morphological characterization of L1-VLPs. (**A**) TEM image of purified L1-VLPs. Scale bar: 200 nm. (**B**) STEM images of the L1-VLPs after concentration by spin filtration. Scale bar: 500 nm.

To shield L1-VLP protein epitopes and facilitate subsequent functionalization of the nanoparticle surfaces with HIV-1 Env trimers, we established a coating of L1-VLPs with a silica shell. To achieve this, we first performed electrostatic colloidal stabilization of the VLPs by adsorbing the polycationic electrolyte PEI onto the negatively charged L1-VLPs.

The silica shell was then deposited by controlled hydrolysis of TEOS, as described previously [19], resulting in L1-SiO_2 NPs (**Figure 2A**).

View Article Online
DOI: 10.1039/D5BM01792K

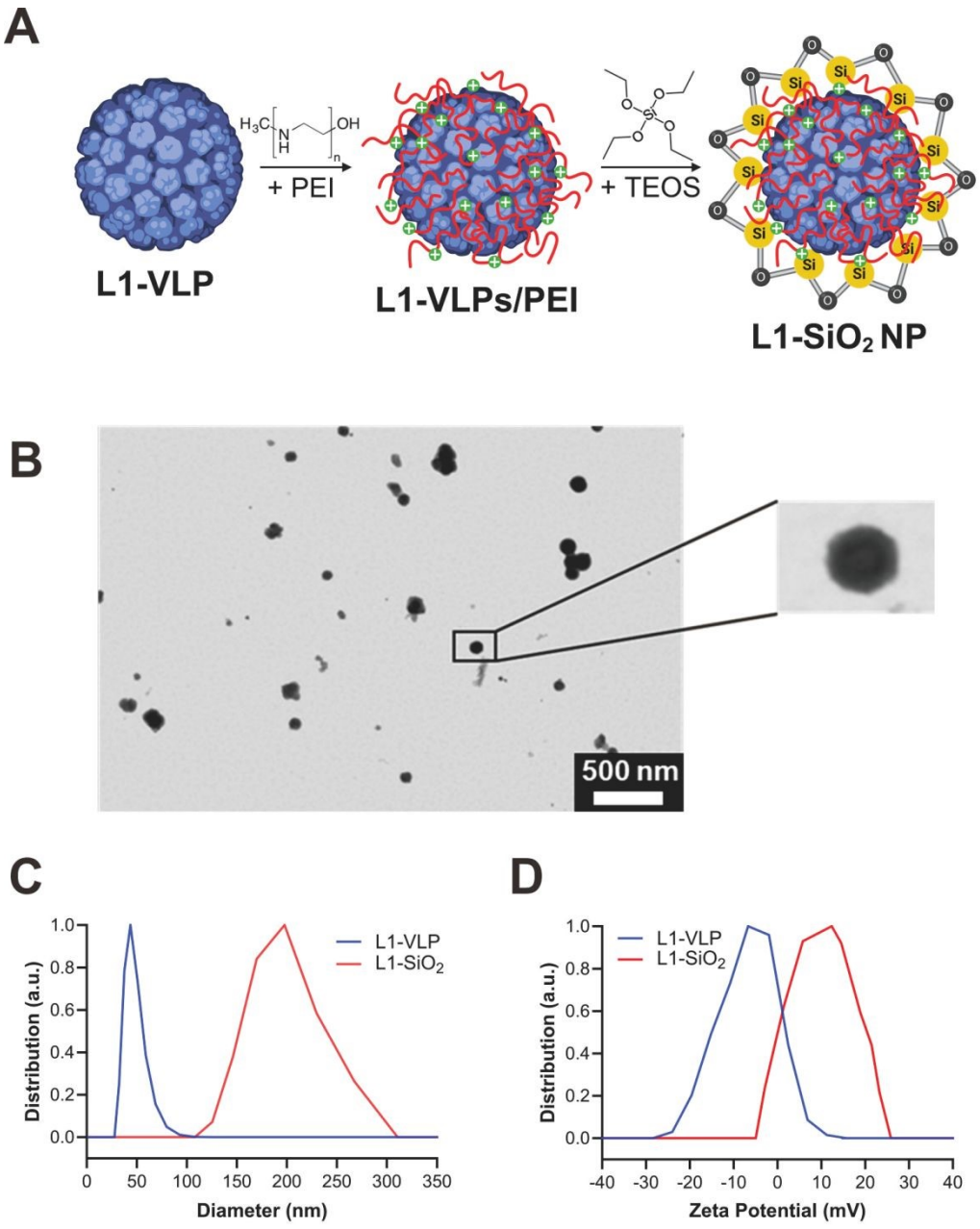

Figure 2. Characterization of L1-SiO_2 NPs. (**A**) Schematic illustration of the synthesis steps for the coating of PEI and silica shell of the VLP surface. Created with BioRender.com (**B**) STEM image of L1-SiO_2 NPs. Scale bar: 500 nm. Relative particle (**C**) size and (**D**) zeta potential distribution (in arbitrary units (a.u.)) of L1-VLPs (in blue) and L1-SiO_2 NPs (in red) measured by DLS.

STEM imaging showed the spherical morphology of the silica-coated L1-VLPs with an average diameter of 197 ± 10 nm (measured by ImageJ) (**Figure 2B**). The hydrodynamic diameter and zeta potential of the L1-SiO_2 NPs were subsequently determined by DLS.

View Article Online
DOI: 10.1039/D5BM01792K

Besides increase in particle size after the silica coating, colloidal stabilization with PEI changed the charge of the L1-SiO_2 NPs (**Figure 2C, D**). A summary of all performed measurements is presented in **Table 1**.

Table 1: Analytical data for L1-VLPs and L1-SiO_2 NPs.

Sample	Diameter* (nm)	Hydrodynamic diameter** (nm)	PDI**	Zeta potential** (mV)
L1- VLP	53 ± 7	63	0.18	-7
L1- SiO_2	197 ± 10	201	0.35	+13

* by STEM; ** by DLS

Energy-dispersive X-ray spectroscopy mapping (**Figure 3**) was carried out to investigate the elemental composition of the L1-SiO_2 NPs. The presence of silicon (blue**, Figure 3B**) and oxygen (green, **Figure 3C**) confirmed the formation of a silica shell around the L1-VLPs. Furthermore, a cross-sectional elemental distribution analysis across a single particle (**Figure 3D**) indicated that the L1-SiO_2 NPs were homogeneously coated with the silica shell, causing the shielding of the scaffold L1 B-cell epitopes.

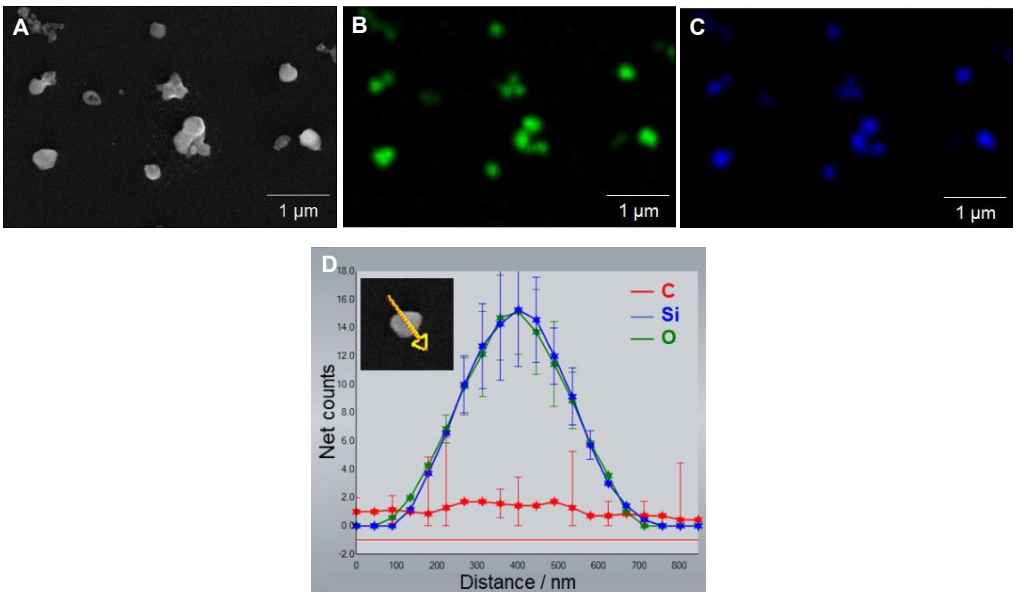

Figure 3. EDX mapping of the L1-SiO_2 NPs. (A) L1-SiO_2 NPs image. (B) The presence of silicon (blue). (C) The presence of oxygen (green). (D) Example of a L1-SiO_2 NP cross-section and elemental EDX line scan of the L1-SiO_2 NPs.

View Article Online
DOI: 10.1039/D5BM01792K

One batch of L1-SiO_2 NPs was produced with fluorescently labeled PEI (PEI-Cy5) for L1-VLP colloidal stabilization. These fluorescent L1-(Cy5)SiO_2 NPs were used to qualitatively assess particle integrity during intracellular accumulation in HeLa cells after *in vitro* co-incubation. As shown in Figure 4a and 4d, the presence of distinct Cy5 (magenta) fluorescence within the cells confirms the stability of the internalized L1-(Cy5)SiO_2 NPs under cell culture conditions.

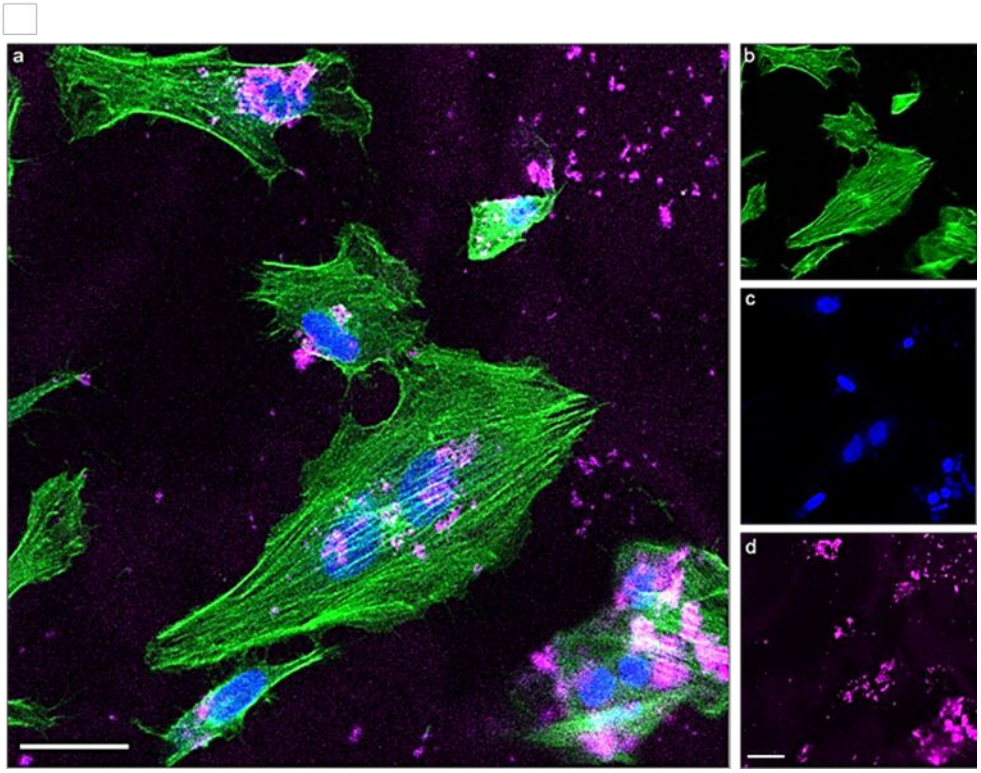

Figure 4. CLSM image of HeLa cells after 24 h incubation with L1-(Cy5)SiO_2 particles. (**a**) Overlay image, (**b**) actin staining with AF488-phalloidin, (**c**) cell nucleus with Hoechst-3342, (**d**) PEI-Cy5 fluorescence. Scale bar: 20 µm.

3.2 L1 epitope shielding *in vivo*

To address the question of the L1 epitope masking efficiency of the silica shell *in vivo*, we performed an experiment in WT mice. To model the presence of pre-existing anti-L1 antibodies, mice received two pre-immunizations with the Cervarix® HPV bivalent vaccine at weeks 0 and 4. Subsequently, the mice were divided into three groups and were immunized with L1-VLPs, L1-SiO_2 NPs, or PBS at weeks 10 and 14 (**Figure 5A**). Serum samples were collected at multiple time points to measure L1 antibody levels post-immunization, aiming to assess the potential masking effect of the silica shell.

View Article Online
DOI: 10.1039/D5BM01792K

Quantification of anti-L1 antibodies in serum by ELISA demonstrated that antibody levels in mice peaked within a few weeks following two pre-immunizations with Cervarix® (**Figure 5B**). Following this initial peak, antibody levels in the PBS control group gradually declined, reflecting the natural waning of antibody production once the antigen was no longer present. In the group boosted with L1-VLPs, antibody levels remained elevated, indicating reactivation of the immune response in the presence of the antigen (**Figure 5B**). In contrast, the group boosted with L1-SiO_2 NPs showed an antibody level trend similar to that of the PBS control group, suggesting that the silica coating of L1-VLPs effectively masked the L1 antigen *in vivo* (**Figure 5B**).

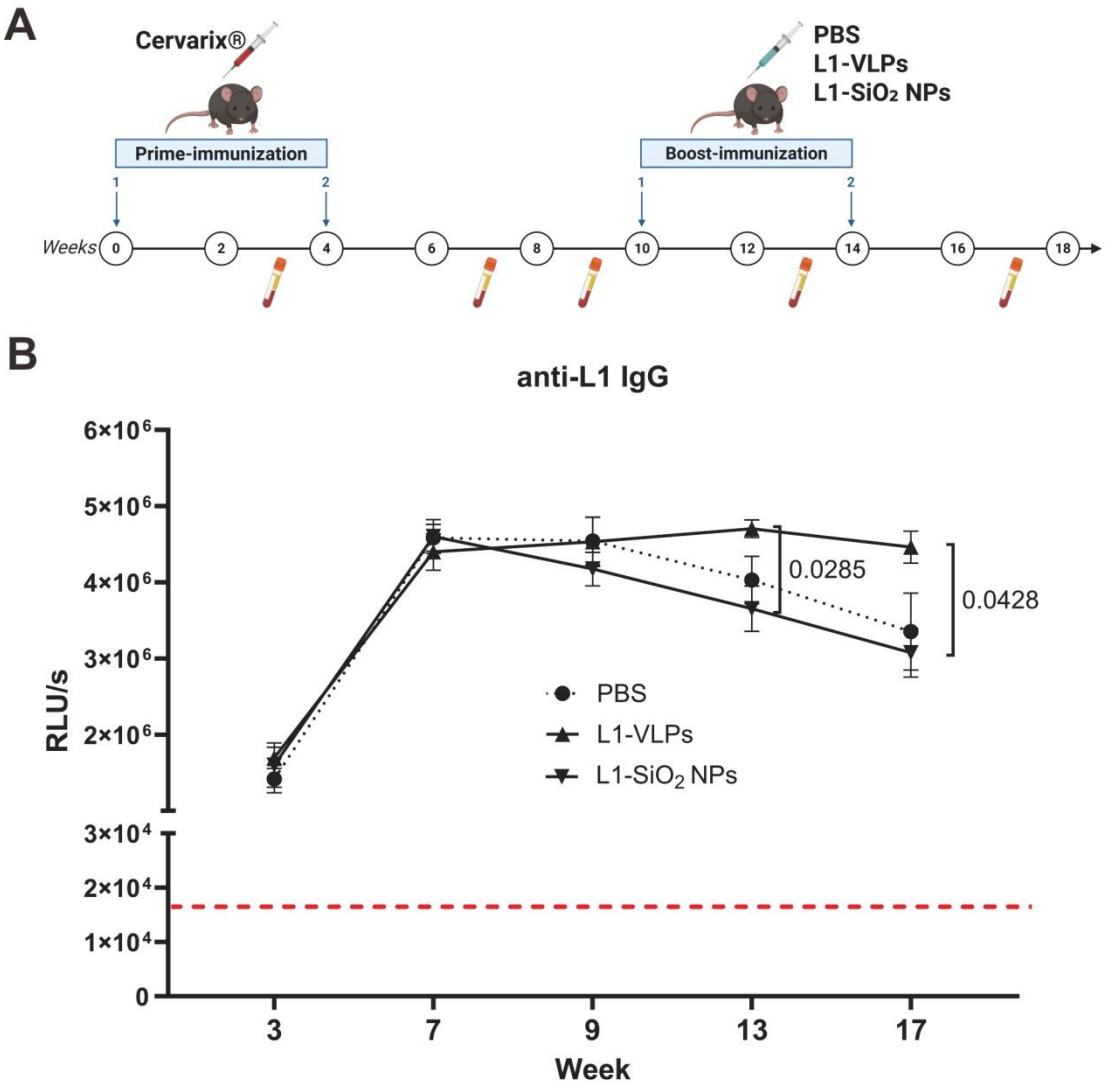

Figure 5. SiO_2 shielding of L1 NP epitopes *in vivo*. (A) Immunization scheme. Created with BioRender.com. Mice (3 groups, *n* = 6 per group) were pre-immunized twice intramuscularly with Cervarix® HPV bivalent vaccine (1:20 dilution, on week 0 and week 4). On week 10 and 14 mice were boosted either with PBS or L1-VLPs or L1-SiO_2 NPs

(both contained 2µg/ml L1). (B) Anti-L1 IgG immune response. The dashed red line represents the background of naive sera for anti-L1 antibodies. Data presented as Mean ± SEM; statistically significant differences between L1 NPs and L1-SiO_2 NPs were observed at week 13 (p = 0.0285; Ordinary one-way ANOVA, multiple comparison) and at week 17 (p = 0.0428; Ordinary one-way ANOVA, multiple comparison).

View Article Online
DOI: 10.1039/D5BM01792K

3.3 Functionalization of L1-SiO_2 with Env trimers

We [16, 20] and others [21] demonstrated that NPs with oriented display of HIV-1 Env trimers on the surface enhance B cell activation and antibody production more efficient than NPs with randomly conjugated Env trimers. Previously, we developed a method for orthogonal covalent coupling of Env trimers to biodegradable calcium phosphate NPs via genetically encoded aldehyde-tags and confirmed that this method does not diminish Env antigenicity and pre-fusion conformation [16]. Since the silica shell can be covalently modified using well-established siloxane chemistry [19], we functionalized L1-SiO_2 NPs with 3-(azidopropyl)triethoxysilane, thereby introducing reactive azide groups onto their surface as described previously [22]. These azide groups facilitate covalent attachment to Env trimers via click chemistry (**Figure 6A**).

View Article Online
DOI: 10.1039/D5BM01792K

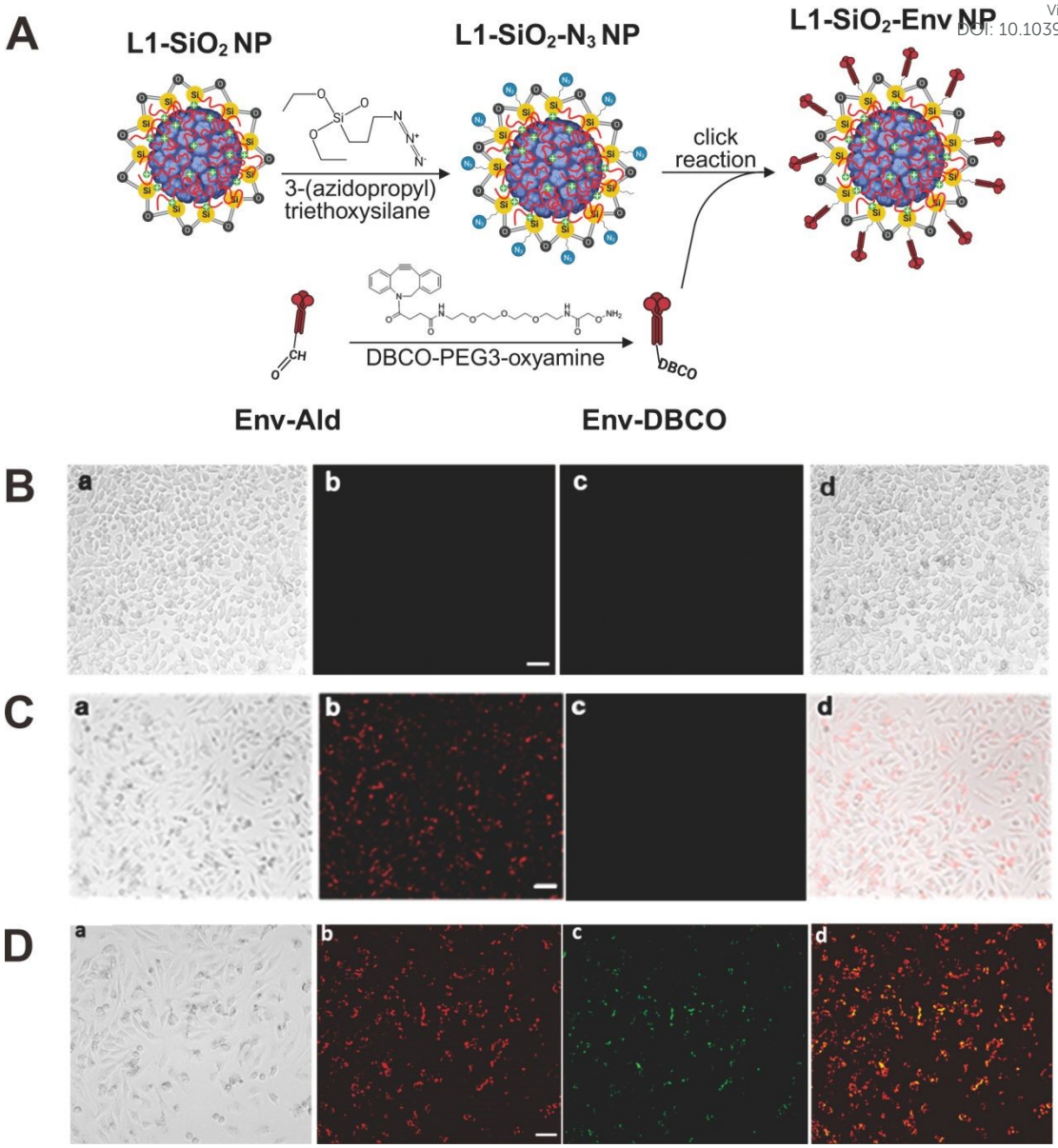

Figure 6. (**A**) Surface functionalization of L1-SiO_2 NPs with Env trimers via click chemistry. Created with BioRender.com. L1-VLPs coated with polyethyleneimine (PEI) and silica (SiO_2) were functionalized with 3-(azidopropyl)triethoxysilane to introduce azide (N_3) groups on the particle surface. Separately, HIV-1 Env trimers bearing aldehyde groups (Env-Ald) were modified with DBCO-PEG_3-oxyamine to generate DBCO-functionalized Env (Env-DBCO). A copper-free strain-promoted azide–alkyne cycloaddition (SPAAC) click reaction enabled covalent attachment of Env trimers to the azide-modified NPs. (**B-D**) Fluorescence microscopy of HeLa cells after 24 h incubation with (**B**) soluble Env-AF488 (control), (**C**) L1-(Cy5)SiO_2 NPs and (**D**) L1-(Cy5)SiO_2-Env(AF488) NPs. In (**a**) the cells in the brightfield, in (**b**) PEI-Cy5, in (**c**) Env-AF488 and in (**d**) the overlay. Scale bar: 50 µm.

In order to analyze efficiency of the Env trimer coupling and *in vitro* stability of the L1-SiO_2-

Env NPs, we synthesized a batch of fluorescently labelled NPs. To this end, we used fluorescent PEI-Cy5 molecules for L1-VLP colloidal stabilization and conjugated the functionalized silica shell with fluorescently labelled Env-trimers (Env-AF488), that resulted in L1-(Cy5)SiO_2-Env(AF488) double labelled NPs. This allowed to determine the concentration of PEI-Cy5 and Env-AF488 molecules and to derive an estimate of 48 Env-AF-488 trimer molecules per NP (**Table 2**).

Table 2: Concentration and molecule count of PEI and Env in NP preparations.

Sample	PEI-Cy5 (kg / m^{-3})	Env-AF488 (kg / m^{-3})	NP (number* per m^{-3})	PEI-Cy5 (number* per NP)	Env-AF488 (number* per NP)
L1-(Cy5)SiO_2	0.132	-	$2.25 \cdot 10^{19}$	141	-
L1-(Cy5)SiO_2-Env(AF488)	0.118	0.670	$2.01 \cdot 10^{19}$	142	48

* number of corresponding molecules

To assess the stability of Env conjugation under biologically relevant cell culture conditions , we cultivated HeLa cells with L1-(Cy5)SiO_2 and L1-(Cy5)SiO_2-Env(AF488) NPs. HeLa cells served as a robust adherent model system for visualizing nanoparticle integrity and conjugate stability under controlled *in vitro* conditions. After 24 hours of co-incubation fluorescence microscopic images were taken (**Figure 6B-D**). Since soluble (non-conjugated) Env-AF488 trimers do not provide detectable intracellular signals under these conditions (**Figure 6B**), the fluorescence overlay of the Cy5 and AF488 signals indicates stable physical co-localization of the nanoparticle scaffold and the conjugated Env trimers (Figure **6D**). This persistent co-localization was further corroborated by confocal laser scanning microscopy (Figure 7), demonstrating the stability of the Env conjugation during intracellular accumulation.

View Article Online
DOI: 10.1039/D5BM01792K

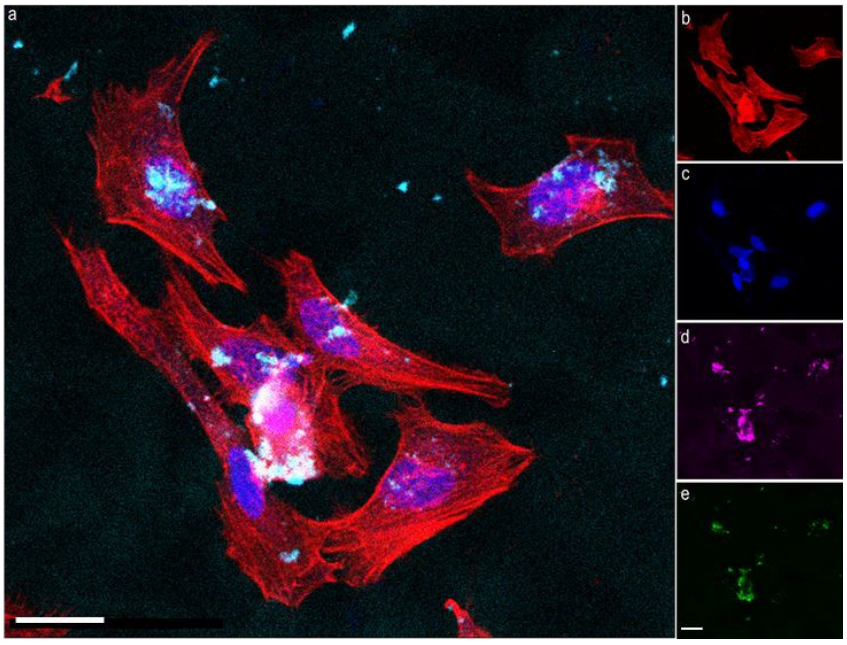

Figure 7. CLSM image of HeLa cells after 24 h incubation with L1-(Cy5)SiO_2-Env(AF488) NPs. In (a) the overlay image, in (b) actin staining with AF568-phalloidin, (c) cell nucleus with Hoechst-3342, (d) PEI-Cy5 fluorescence and in (e) Env-AF488. Scale bar: 20 µm.

3.4 Activation of Env-specific B cells by L1-SiO_2-Env *in vitro*

Chemical modifications of silica films enable their surfaces to load heterologous antigens, providing a versatile platform for immunological studies. In this study, azide groups were introduced onto the L1-SiO_2 surface to facilitate the covalent attachment of Env-DBCO via click chemistry. This method ensures a stable and precise coupling, allowing the repetitive display of Env proteins on the nanoparticle surface. Such a configuration is hypothesized to enhance the activation of Env-specific B cells via the crosslinking of B cell receptors (BCRs), a critical step for effective immune activation. To investigate this, *in vitro* B cell activation experiments were performed to confirm the high-density and functional display of Env trimers on L1-SiO_2 NPs. Env-specific B cells were isolated from BCR-transgenic PGT121 mice, which express receptors specific to the Env antigen, while WT B cells were used as a comparative control. These B cells were incubated with a range of L1-SiO_2-Env nanoparticle concentrations (1–100 ng/mL Env), allowing for a detailed dose-response analysis. As negative controls, non-coupled Env trimers mixed with or without L1-SiO_2 were used to rule out unspecific effects unrelated to BCR crosslinking. LPS was included

View Article Online
DOI: 10.1039/D5BM01792K

as a positive control to provide a benchmark for polyclonal activation of B cells through receptor-independent pathways. After 18 hours of incubation, B cell viability and activation were assessed using flow cytometry, focusing on the expression of CD86, a key activation marker. Under resting conditions, naïve B cells express CD86 at low levels. However, upon antigenic stimulation via BCR engagement or polyclonal activation through LPS, CD86 is markedly upregulated. The L1-SiO_2-Env NPs induced a dose-dependent increase in CD86 expression in Env-specific B cells, with the strongest response observed at the highest concentration tested (100 ng/mL Env; **Figure 8A**). Interestingly, high concentrations of uncoupled L1-SiO_2 NPs led to a minor increase in CD86 expression, a nonspecific effect also observed in wild-type B cells (**Figure 8B**). These findings suggest that while L1-SiO_2 NPs can elicit some nonspecific interactions with BCRs, the robust activation observed with Env-specific B cells is largely antigen-dependent. This conclusion is supported by related studies, which have noted similar nonspecific interactions between silica-based NPs and BCRs [23]. To further characterize B cell activation, CD40 expression on activated B cells was additionally assessed. CD40 is a key costimulatory receptor required for T cell–dependent B cell responses, including germinal center formation, immunoglobulin class switching, and affinity maturation through interaction with CD40L expressed on activated $CD4^+$ T cells [24]. The proportion of $CD86^+CD40^+$ cells among Env-specific and WT B cells was therefore quantified after stimulation with L1-SiO_2-Env NPs (Figure 8C, D). Consistent with the CD86 data, Env-specific B cells displayed a markedly higher frequency of $CD86^+CD40^+$ cells compared with WT B cells, indicating antigen-dependent activation of Env-specific B cells. B cell viability of the Env-specific B cells remained unaffected across the tested L1-SiO_2-Env concentration range (Figure 8E). Overall, the results demonstrate the successful engineering of L1-SiO_2-Env NPs capable of effectively presenting Env antigens in a high-density, repetitive format that robustly activated Env-specific B cells.

View Article Online
DOI: 10.1039/D5BM01792K

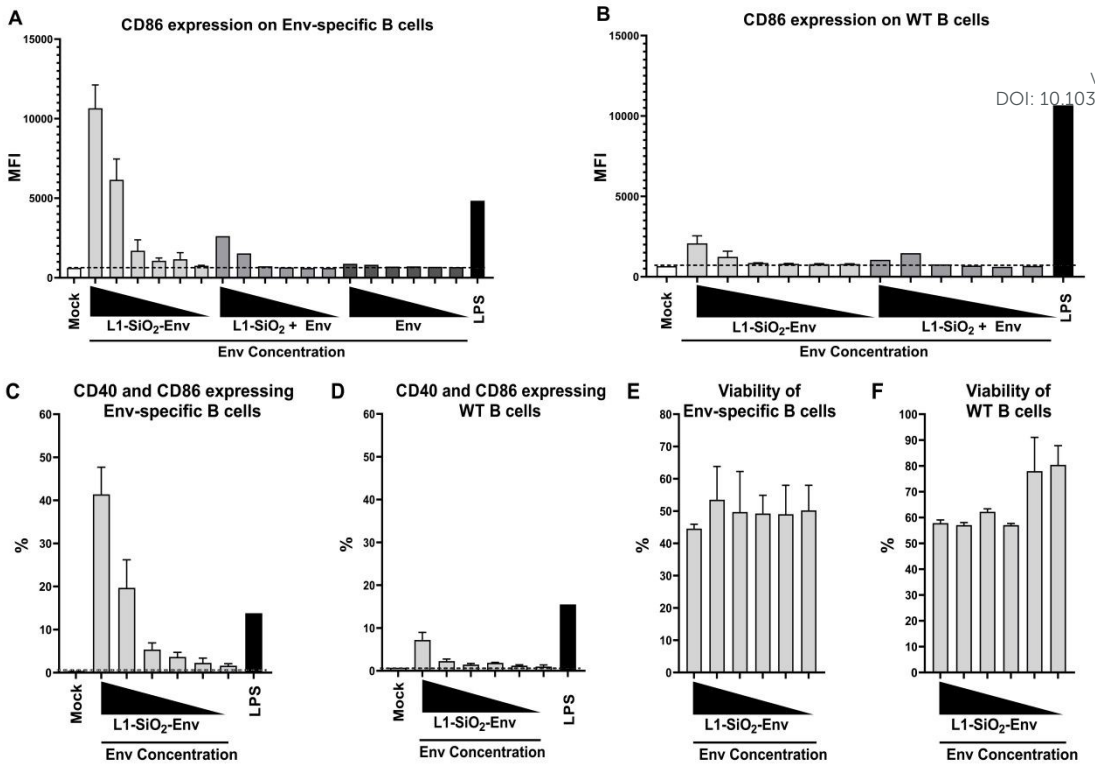

Figure 8. Activation of naïve Env-specific B cells by L1-SiO_2-Env nanoparticles *in vitro*.

Naïve Env-specific (**A**) or wild-type (WT) B cells (**B**) were incubated for 18 hours with L1-SiO_2-Env NPs, or L1-SiO_2 NPs mixed with soluble Env trimers (L1-SiO_2 + Env), or soluble Env trimers alone (Env) at various dilutions normalized to their bulk Env concentration (1–100 ng/mL). Lipopolysaccharide (LPS) 2 µg/mL served as a non-specifically activating positive control. Negative controls included unstimulated (mock) cells. After 18 hours, cells were stained for viability, and B cell activation was assessed by measuring the upregulation of CD86 on CD19+ cells via flow cytometry. Percentage of $CD86^{+}CD40^{+}$ cells among viable CD19 positive (**C**) Env-specific B cells and (**D**) WT B cells after stimulation with mock, L1-SiO_2-Env NPs, or LPS. Viability of CD19 positive (**E**) Env-specific B cells and (**F**) WT B cells after stimulation with increasing concentrations of L1-SiO_2-Env NPs (1–100 ng/mL Env) expressed as percentage of the mock control for Env-specific B cells.

3.4 Humoral immune responses in mice after L1-SiO_2-Env vaccinations

The immunogenic potential of L1-SiO_2-Env NPs was evaluated through the measurement of Env-specific and scaffold-specific IgG responses, providing evidence of the platform's efficiency in presenting antigens to the immune system. As we demonstrated previously, immunization with soluble Env trimers alone was insufficient to induce a robust humoral immune response [15]. In contrast, vaccination with L1-SiO_2-Env NPs resulted in significantly higher anti-Env IgG levels. A single dose of the NPs substantially enhanced antibody

production compared to the control group (**Figure 9A**), and a second dose further amplified this effect, culminating in peak antibody levels.

View Article Online
DOI: 10.1039/D5BM01792K

At the same time, the L1-specific IgG levels in the L1-SiO_2-Env group were exceptionally low, indicating a highly specific immune response directed toward the Env antigen (**Figure 9B**). This observation suggests that the silica coating effectively encapsulated the L1-VLP scaffold, preventing the exposure of L1 epitopes and thereby minimizing the induction of scaffold-specific antibodies. This specificity is of paramount importance, as it reduces potential immune interference by the scaffold, ensuring that the focus of the immune system remains on the target antigen. By contrast, the L1-VLP control group displayed robust L1-specific IgG production (**Figure 9B**), reaffirming the inherent immunogenicity of L1 when directly presented as an antigen.

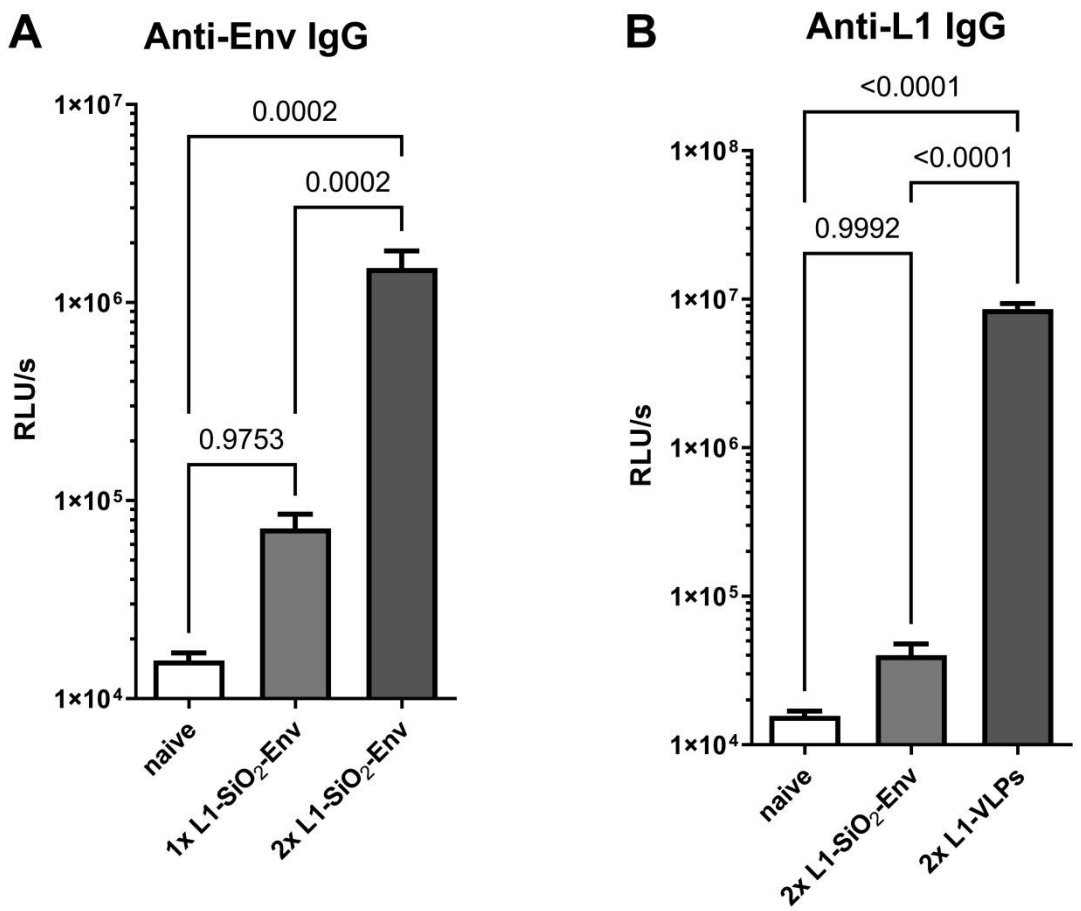

Figure 9. Antibody levels after L1-SiO2-Env immunization.

(**A**) WT mice were immunized with 60 µl L1-SiO_2-Env NPs (0.1µg Env in total) at weeks 0 and 4. Blood samples were drawn at week 3 (1x L1-SiO_2-Env) and 6 (2x L1-SiO_2-Env). (**B**) WT mice were immunized with 60 µL L1 VLPs or L1-

SiO_2-Env NPs (2µg/mL L1 in total) at weeks 0 and 4. Blood samples were drawn at week 6. The relative amount of Env- and L1-specific IgG antibodies in the sera was determined using serum ELISA and is expressed as relative light units per second (RLU/s). Statistical significance was assessed using the ordinary one-way ANOVA, multiple comparison test.

View Article Online
DOI: 10.1039/D5BM01792K

Shielding of the L1 scaffold facilitates Env immune responses in HPV immunized mice.

To further validate that Env delivered by L1-SiO_2 influences the production of specific antibodies due to the shielding effect of the scaffold, we optimized the immunization strategy in a mouse model. The experimental groups received two doses of the licensed L1-based HPV vaccine Cervarix® at week 0 and 4, while the control group was injected with PBS. Subsequently, both groups were immunized with a one dose of L1-Env or L1-SiO_2-Env (**Figure 10A**). In the mice immunized with L1-Env serum analysis revealed a trend to lower levels of Env-specific antibodies in the experimental group pre-vaccinated with Cervarix® compared to the PBS group (**Figure 10B**). This suggests that the pre-existing L1-specific immune response attenuated the Env-specific immune response. In contrast, mice that were immunized with L1-SiO_2-Env displayed the opposite trend. Specifically, the group pre-vaccinated with Cervarix® exhibited higher levels of Env-specific antibodies in their serum compared to the PBS control group (**Figure 10C**). This outcome suggests that the shielding of the L1 scaffold with the silica shell demonstrated above (Figure 5B) supports antibody response to the conjugated Env antigen in animals, previously vaccinated against HPV.

View Article Online
DOI: 10.1039/D5BM01792K

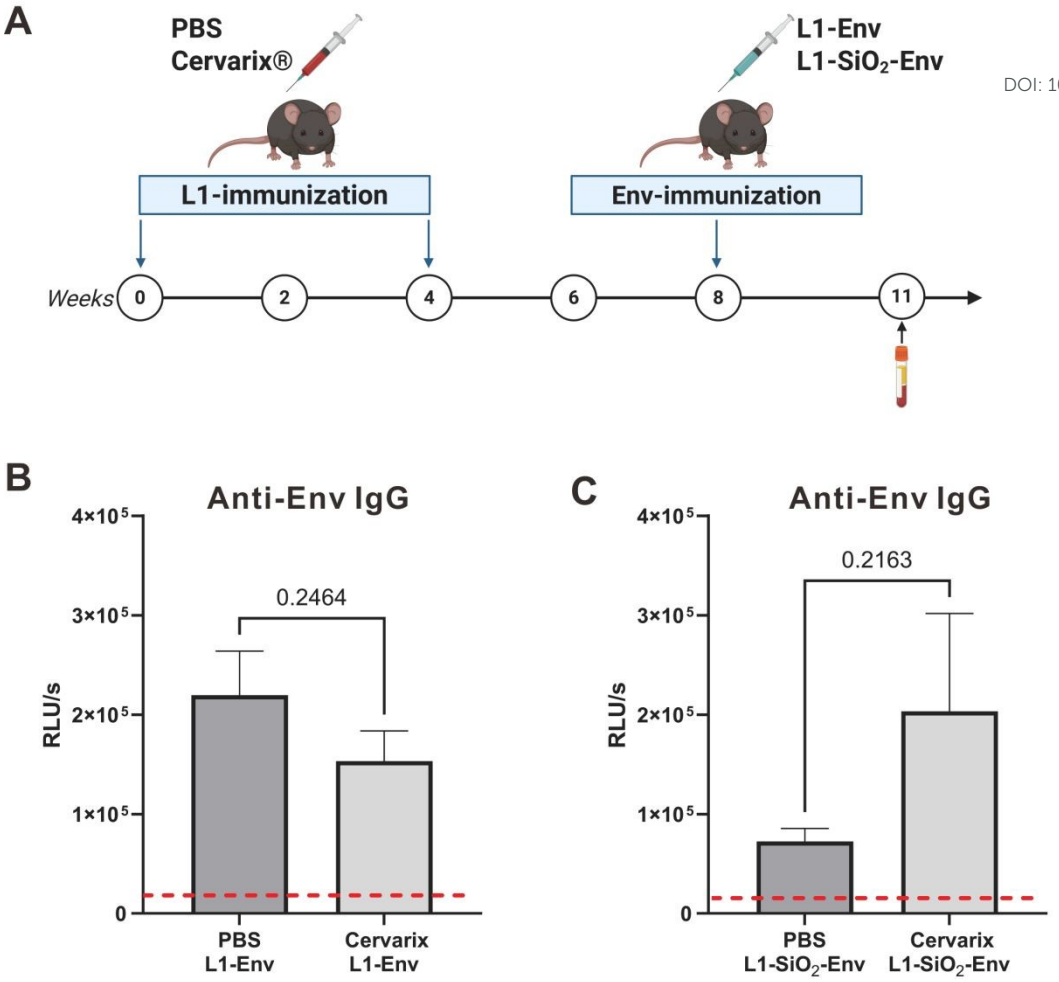

Figure 10. Env immune responses in HPV immunized mice. (**A**) Immunization scheme. Created with BioRender.com. Wt mice (3 groups, n=6 per group) were pre-immunized twice intramuscular with PBS or with Cervarix® HPV bivalent vaccine (1:20 dilution, on week 0 and week 4). On week 8 mice were boosted either with L1-Env NPs or with L1-SiO_2-Env NPs (both contained 2µg/ml Env). Blood samples were drawn at week 11. The relative amounts of Env-specific IgG antibodies in the sera of L1-Env (**B**) and L1-SiO2-Env (**C**) immunized mice were determined using serum ELISA and is expressed as relative light units per second (RLU/s). Statistical analysis was assessed using two-tailed unpaired *t-test*. The dashed red line represents the background of naive sera for anti-L1 antibodies. Data presented as Mean ± SEM;

4. Discussion

Self-assembling natural proteins form stable, symmetric NPs (10–150 nm), a size ideal for immune cell interaction [25]. These nano-scaffolds can be engineered to present ordered immunogen arrays for vaccine design, providing notable benefits over other multivalent

View Article Online
DOI: 10.1039/D5BM01792K

antigen presentation platforms [6]. A recurring challenge in chimeric vaccine design, however, are the inhibitory effects of scaffold-specific antibody responses: scaffold-directed humoral memory may lead to antibody-mediated clearance of the vaccine material, potentially limiting the effectiveness of sequential immunizations [26, 27].

Following the 1992 discovery of the self-assembling and highly immunogenic properties of HPV L1-VLPs [28], these nano-structures have been extensively examined for vaccine development. This effort resulted in VLP-based HPV vaccines that are used world-wide. Furthermore, the versatility of the L1-VLP scaffold has been exploited to create hybrid VLP vaccine candidates displaying heterologous (non-HPV) antigens [29-31].

We recently demonstrated that L1-VLPs conjugated with stabilized HIV-1 Env trimers (L1-Env NPs) efficiently activate Env-specific B cells via B cell receptor engagement and induce both Env- and L1-specific antibody responses in mice without adjuvant. Notably, L1-Env NPs elicited significantly higher Env-specific antibody levels compared to a mixture of Env trimers and uncoupled L1-VLPs. While we observed partial shielding of L1 epitopes by the conjugated Env trimers, resulting in reduced L1-specific antibody responses [15], the extent of shielding appears to depend on antigen characteristics. For example, insertion of a HIV-1 CTL epitope with a length of 10 amino acids into the HPV L1 capsid did not affect anti-L1 antibody induction after immunization [30], suggesting that size and glycosylation of the antigen might play a role. Additionally, the antigen density on the nanoparticle scaffold may diminish anti-scaffold responses. However, even a high-density display of respiratory syncytial virus pre-fusion glycoprotein trimers on I53-50 NPs did not sterically prevent antibody access to the scaffold [32], and maximizing the circumsporozoite protein density on a hepatitis B virus scaffold only partially reduced anti-scaffold antibody responses [33].

The accessibility of L1-specific antibodies to the L1-VLP core raises a question about the impact of pre-existing anti-HPV (anti-scaffold) immune responses, particularly given the global implementation of HPV vaccination schedules. This concern is supported by well-documented effects of vector or carrier immunity in various vaccine platforms. For example, pre-existing antibodies to adenovirus serotype-5 (Ad5) are known to impede the efficacy of Ad5-based vaccines, leading to significantly reduced immunogen-specific responses in

View Article Online
DOI: 10.1039/D5BM01792K

seropositive individuals [26]. Likewise, repeated use of the same protein carrier in conjugate vaccines can suppress responses against the hapten antigen [27]. Consistent with this concern, we observed in the current study that direct Env conjugation to L1-VLPs attenuated Env-specific responses in HPV pre-immunized animals (**Figure 10B**). This observation aligns with findings from a study using Env-ferritin NPs, which also reported a negative interference of pre-existing anti-scaffold responses with anti-Env responses [34].

To physically shield the L1-VLP scaffold from pre-existing anti-L1 antibodies, we employed a coating of amorphous silica on the L1-VLPs. This method was initially developed for stabilizing biocompatible calcium phosphate NPs [35]. When administered to mice with high levels of anti-HPV antibodies, these L1-SiO_2 NPs demonstrated remarkable stealth features *in vivo* (**Figure 5**). Two pre-vaccinations with Cervarix® rapidly increased L1 antibody concentration as measured by ELISA, indicating a strong primary immune response (Figure 5B). Following the initial peak, antibody levels gradually declined, as the immune system doesn't sustain high antibody levels indefinitely once the antigen is no longer present. This reduction in antibody concentration, particularly noticeable in the PBS control group after week 9, is a well-documented aspect of immune homeostasis, where antibodies decrease as the antigenic stimulus dissipates. When the mice were re-exposed to the antigen, memory B cells formed during the primary immune response were reactivated, leading to a renewed production of antibodies. This phenomenon was clearly observed in the group boosted with L1-VLPs (**Figure 5B**), where antibody levels remained elevated, indicating an effective recall response by the immune system (also known as an anamnestic response). This response exemplifies the role of immunological memory, which allows for rapid and enhanced antibody production upon subsequent exposure to the same antigen. Crucially, we observed a complete absence of an anamnestic response after the subsequent boost with L1-SiO_2 NPs, strongly indicates that the silica coating remains intact and functionally shields L1 epitopes under physiological conditions from recognition by L1-specific memory B cells [36]. Consistent with the shielding data presented in Figure 5, the absence of substantial *de novo* L1-specific antibodies after two L1-SiO_2-Env immunizations (Figure 9B), further supports the conclusion that the silica shell maintains its structural and functional integrity *in vivo* after chemical modification and

antigen coupling.

View Article Online
DOI: 10.1039/D5BM01792K

Our silica-coating approach offers an alternative to physical masking with polyethylene glycol (PEG, PEGylation), an increasingly utilized tool in pharmaceuticals and biomedicine for similar purposes [37, 38]. Indeed, PEGylation of protein nanoparticle scaffolds like ferritin [39] and I53_dn5 [13] has been shown to dampen anti-scaffold antibody responses, and PEGylated adenoviruses were protected from antibody neutralization in the lungs of mice with high antibody titers to adenovirus [40]. However, recent findings indicate that PEG-specific antibodies can be induced or boosted by vaccination with licensed mRNA vaccines against COVID-19 that contain PEG for stabilization of the lipid NPs [41]. These pre-existing anti-PEG antibodies could negatively impact the reactogenicity of PEG shielded NP vaccines [37].

The possibility of nonspecific immune activation by silica nanoparticles has been reported and therefore warrants consideration [42]. At sufficiently high concentrations, silica nanoparticles can induce pro-inflammatory responses in innate immune cells. However, immunotoxicity appears to be dose-dependent, and silica nanoparticles have been reported to exhibit minimal immunotoxic effects at lower doses (≤ 8 mg/kg) comparable to those used for nanocarrier systems in clinical nanomedicine [43]. Consistent with these observations, the amorphous silica formulation used here has previously been shown to exhibit a favorable biocompatibility profile without detectable cytotoxicity or nonspecific innate immune activation at relevant concentrations [44]. This is in agreement with the minimal activation observed in wild-type B cells *in vitro* (**Figure 8 B, D**). Thus, the robust Env-specific B cell activation (**Figure 8 A, C**) and the targeted Env-specific humoral responses observed *in vivo* (**Figure 9**) are most consistent with antigen-specific activation driven by multivalent Env display rather than nonspecific silica-mediated immune stimulation. Beyond its shielding properties, the silica shell offers the key advantage of enabling covalent modification through siloxane chemistry [19]. We previously developed and validated a method for highly selective bio-conjugation of conformational Env trimers to the surface of inorganic NPs coated with a silica layer [16]. As demonstrated in our *in vitro* assays, the L1-SiO_2-Env NPs effectively activate Env-specific PGT121 B cells (**Figure 8 A, C**). This activation is consistent with the multivalent presentation of engineered BG505-

View Article Online
DOI: 10.1039/D5BM01792K

NFL2P Env trimers, which have been designed to mimic the native prefusion viral spike [17]. Since PGT121 recognition depends on the N332 glycan supersite, the observed activation of PGT121 B cells serves as functional evidence this glycan-dependent epitope remains preserved and accessible after nanoparticle conjugation [45]. Although site-specific coupling involves an oxime ligation step under mildly acidic conditions (pH 4.5), previous characterization demonstrated preservation of Env conformational epitopes. In particular, binding to quaternary and glycan-dependent antibodies, including PG9, PG16, PGT145, and 2G12, was maintained after exposure to the ligation environment [16]. Importantly, the orthogonal C-terminal coupling strategy enables controlled orientation of Env trimers on the nanoparticle surface, in contrast to random amine-based conjugation. Anchoring the trimers via their C-terminus favors an outward-facing display and may reduce accessibility of base-proximal, non-neutralizing epitopes that are commonly immunodominant in soluble Env constructs [46]. Such oriented multivalent display increases local antigen density and promotes efficient BCR cross-linking, a key determinant of B cell activation [20]. Thus, by combining the oriented display of stabilized Env trimers with the physical shielding of the L1 scaffold, our platform is designed to reduce scaffold-directed responses while favoring recognition of relevant neutralizing epitopes. In addition to the *in vitro* visualization (**Figure 6 and 7**), the stability of the L1-SiO_2-Env nanoparticles after Env conjugation is supported by the immunogenicity data shown in **Figure 9**. Since immunization with uncoupled (soluble) Env trimers (even at higher concentrations) does not induce detectable antibody responses [15], the significant increase in Env-specific IgG levels (Figure 9A) indicates that the covalent coupling of Env to the L1-SiO_2 nanoparticles remains sufficiently stable *in vivo* to enable effective B cell activation. The hybrid L1-SiO_2 nanoparticle design differs from previously described silica-based antigen delivery systems in several aspects. In contrast to purely inorganic silica nanoparticles, which typically rely on adsorption or encapsulation of antigens within an inert inorganic matrix [47, 48], the present platform retains a self-assembled viral protein scaffold while introducing a thin silica shell that modulates immune accessibility and enables controlled surface functionalization. Previous studies, including work by Peterhoff and colleagues [49], demonstrated that Env trimers can be directly conjugated to solid silica nanoparticles, resulting in preserved antigenicity and Env-specific antibody induction. However, these systems rely on entirely inorganic cores. In contrast,

View Article Online
DOI: 10.1039/D5BM01792K

our hybrid architecture retains a full-length licensed VLP scaffold containing multiple $CD4^+$ T cell epitopes, which may become particularly relevant in the context of pre-existing immunity. As shown in Figure 10,

L1-SiO_2-Env vaccination of mice pre-immunized against HPV enhanced Env-specific antibody production compared to non-vaccinated animals (**Figure 10C**). This observation can be attributed to the recruitment of heterologous T-cells providing intrastructural help (ISH), a mechanism initially described in the context of influenza virus [50] and later extended to HIV-1 VLPs [51] and synthetic [52, 53] nanoparticle vaccines. ISH modulates humoral immunity by exploiting pre-existing cellular immunity against heterologous epitopes. This concept suggests the design of NPs displaying the immunogen of choice on their surface and containing efficacious T helper cell epitopes from licensed vaccines internally. B cells specific for the surface antigen internalize the entire nanoparticle via BCR and subsequently present the encapsulated peptide epitopes to T helper cells previously induced by licensed vaccines [54]. With L1-Env NPs, however, any potential ISH from L1-specific T cells was likely overshadowed by the dominant effect of L1-specific antibodies. Therefore, when pre-existing anti-scaffold immunity is present, effective shielding of the protein scaffold might be a crucial prerequisite for ISH to exert a noticeable effect.

Overall, considering the potential of ISH to modulate humoral immune responses and its implications for clinical translation, the fact that L1-SiO_2-Env NPs contain the full-length L1 antigen from licensed HPV vaccines—rather than MHC class II haplotype-restricted single epitopes—presents an advantage over homogeneous silica NPs conjugated with Env trimers [55] or other Env-carrying synthetic NPs loaded only with selected epitopes [52, 53]. However, this potential advantage warrants further evaluation through direct side-by-side comparison studies.

5. Conclusion

In summary, this study introduces a novel HIV-1 vaccine strategy employing silica-coated

DOI: 10.1039/D5BM01792K

HPV L1-VLPs functionalized with HIV Env trimers to overcome limitations associated with pre-existing anti-scaffold immunity. The silica shell effectively shielded L1 epitopes *in vivo*, preventing recognition by L1-specific memory B cells. Notably, L1-SiO_2-Env vaccination enhanced Env-specific antibody production in HPV pre-immunized mice, suggesting the involvement of ISH provided by the full-length L1 antigen. Overall, L1-SiO_2-Env NPs present a promising platform for HIV-1 vaccine development by integrating effective scaffold shielding, stable antigen display, and the potential for harnessing pre-existing scaffold immunity through ISH. This silica-coating approach can be readily applied to other protein-based nanoparticle scaffolds to mitigate challenges arising from pre-existing immunity against those scaffolds.

Competing interests

The authors declare that they have no competing interests.

Funding

This research was funded by the Deutsche Forschungsgemeinschaft (DFG, German Research Foundation) - 432828510 (EP 22/55-1; TE 1195/3–1 and UE 45/21–1) and the Staedtler Stiftung (Nuremberg, Germany).

Authors' Contributions

Conceptualization, M.E., V.T. and K.Ü.; methodology, D.D., M.E. and V.T.; investigation, Y.W., K.K., N.B., K.L. C.W. and P.A.; formal analysis, Y.W., K.K., D.D. and V.T.; data curation, M.E., V.T., K.Ü; writing - original draft, Y.W. and V.T.; writing - review and editing, M.E., K.K. and K.Ü.; visualization, Y.W., K.K., K.L. and P.A.; supervision, D.D., V.T., K.Ü.; project administration, M.E., V.T.; funding acquisition, M.E., V.T. and K.Ü.

All authors read and approved the final manuscript.

Acknowledgement

View Article Online
DOI: 10.1039/D5BM01792K

We thank Michel Nussenzweig (The Rockefeller University, New York, NY, USA) for PGT121 mice donation and Fondation Dormeur (Vaduz) for financially supporting the acquisition of the Zetasizer device.

Data Availability

The data that support the findings of this study are available from the corresponding author upon reasonable request.

References

1. P. D. Kwong, J. R. Mascola and G. J. Nabel, *J Int AIDS Soc*, 2012, **15**, 17407.

2. A. C. Boomgarden and C. Upadhyay, *Vaccines (Basel)*, 2025, **13**.

3. N. S. Greenspan, *Front Immunol*, 2014, **5**, 335.

4. V. A. Adepoju, D. C. Udah, O. I. Onyezue, Q. E. S. Adnani, S. Jamil and M. N. Bin Ali, *Vaccines (Basel)*, 2025, **13**.

5. J. Kim, S. Vasan, J. H. Kim and J. A. Ake, *J Int AIDS Soc*, 2021, **24 Suppl 7**, e25793.

6. J. Lopez-Sagaseta, E. Malito, R. Rappuoli and M. J. Bottomley, *Comput Struct Biotechnol J*, 2016, **14**, 58-68.

7. L. Treuel, X. Jiang and G. U. Nienhaus, *J R Soc Interface*, 2013, **10**, 20120939.

8. F. B. Sulczewski, R. B. Liszbinski, P. R. T. Romao and L. C. Rodrigues Junior, *Arch Virol*, 2018, **163**, 2313-2325.

9. M. Zaman, M. F. Good and I. Toth, *Methods*, 2013, **60**, 226-231.

10. J. Schiller and B. Chackerian, *PLoS Pathog*, 2014, **10**, e1004254.

11. S. M. Curley and D. Putnam, *Front Bioeng Biotechnol*, 2022, **10**, 867119.

12. L. Vuitika, N. Cortes, V. B. Malaquias, J. D. Q. Silva, A. Lira, W. A. Prates-Syed, L. F. Schimke, D. Luz, R. Duraes-Carvalho, A. Balan, N. O. S. Camara, O. Cabral-Marques, J. E. Krieger, M. H. Hirata and G. Cabral-Miranda, *Sci Rep*, 2024, **14**, 24228.

13. J. C. Kraft, M. N. Pham, L. Shehata, M. Brinkkemper, S. Boyoglu-Barnum, K. R. Sprouse, A. C. Walls, S. Cheng, M. Murphy, D. Pettie, M. Ahlrichs, C. Sydeman, M. Johnson, A. Blackstone, D. Ellis, R. Ravichandran, B. Fiala, S. Wrenn, M. Miranda, K. Sliepen, P. J. M. Brouwer, A. Antanasijevic, D. Veesler, A. B. Ward, M. Kanekiyo, M.

Pepper, R. W. Sanders and N. P. King, *Cell Rep Med*, 2022, **3**, 100780.

14. A. S. Cordeiro, Y. Patil-Sen, M. Shivkumar, R. Patel, A. Khedr and M. A. Elsawy, *Pharmaceutics*, 2021, **13**.

15. Y. Wang, N. Bartelsen, P. Arnold, S. Mueller-Schmucker, C. Weingartner, J. Beutel, J. Eichler, V. Temchura, D. Damm and K. Uberla, *Sci Rep*, 2025, **15**, 32927.

16. D. Damm, K. Kostka, C. Weingartner, J. T. Wagner, L. Rojas-Sanchez, S. Gensberger-Reigl, V. Sokolova, K. Uberla, M. Epple and V. Temchura, *Acta Biomater*, 2022, **140**, 586-600.

17. S. K. Sharma, N. de Val, S. Bale, J. Guenaga, K. Tran, Y. Feng, V. Dubrovskaya, A. B. Ward and R. T. Wyatt, *Cell Rep*, 2015, **11**, 539-550.

18. P. Arnold, P. Himmels, S. Weiss, T. M. Decker, J. Markl, V. Gatterdam, R. Tampe, P. Bartholomaus, U. Dietrich and R. Durr, *Retrovirology*, 2014, **11**, 42.

19. D. Kozlova, S. Chernousova, T. Knuschke, J. Buer, A. Westendorf and M. Epple, *J. Mater. Chem.*, 2011, **22**, 396-404.

20. R. Di Vincenzo, J. Beutel, P. Arnold, Y. Wang, D. Damm, P. Tannig, A. Lux, V. Temchura, J. Eichler and K. Uberla, *Front Immunol*, 2024, **15**, 1344346.

21. D. Peterhoff, S. Thalhauser, P. Neckermann, C. Barbey, K. Straub, J. Nazet, R. Merkl, G. Laengst, M. Breunig and R. Wagner, *Eur J Pharm Biopharm*, 2022, **181**, 88-101.

22. L. Rojas-Sánchez, S. Riebe, J. Voskuhl and M. Epple, *ChemNanoMat*, 2018, **5**.

23. N. Ganesan, S. Ronsmans and P. Hoet, *Front Immunol*, 2022, **13**, 1025028.

24. R. Elgueta, M. J. Benson, V. C. de Vries, A. Wasiuk, Y. Guo and R. J. Noelle, *Immunol Rev*, 2009, **229**, 152-172.

25. D. J. Irvine and B. J. Read, *Curr Opin Immunol*, 2020, **65**, 1-6.

26. W. C. Wang, E. E. Sayedahmed and S. K. Mittal, *Viruses*, 2022, **14**.

27. X. Renjifo, S. Wolf, P.-P. Pastoret, H. Bazin, J. Urbain, O. Leo and M. Moser, *The Journal of Immunology*, 1998, **161**, 702-706.

28. R. Kirnbauer, F. Booy, N. Cheng, D. R. Lowy and J. T. Schiller, *Proc Natl Acad Sci U S A*, 1992, **89**, 12180-12184.

29. K. N. Nand, T. B. Jordan, X. Yuan, D. A. Basore, D. Zagorevski, C. Clarke, G. Werner, J. Y. Hwang, H. Wang, J. J. Chung, A. McKenna, M. D. Jarvis, G. Singh and C. Bystroff, *Vaccine*, 2023, **41**, 6791-6801.

30. C. W. Chen, N. Saubi and J. Joseph-Munne, *Int J Mol Sci*, 2023, **24**.

View Article Online
DOI: 10.1039/D5BM01792K

31. S. Thrane, C. M. Janitzek, M. O. Agerbaek, S. B. Ditlev, M. Resende, M. A. Nielsen, T. G. Theander, A. Salanti and A. F. Sander, *PLoS One*, 2015, **10**, e0143071.

32. J. Marcandalli, B. Fiala, S. Ols, M. Perotti, W. de van der Schueren, J. Snijder, E. Hodge, M. Benhaim, R. Ravichandran, L. Carter, W. Sheffler, L. Brunner, M. Lawrenz, P. Dubois, A. Lanzavecchia, F. Sallusto, K. K. Lee, D. Veesler, C. E. Correnti, L. J. Stewart, D. Baker, K. Lore, L. Perez and N. P. King, *Cell*, 2019, **176**, 1420-1431 e1417.

33. K. A. Collins, R. Snaith, M. G. Cottingham, S. C. Gilbert and A. V. S. Hill, *Sci Rep*, 2017, **7**, 46621.

34. K. Sliepen, E. Schermer, I. Bontjer, J. A. Burger, R. F. Levai, P. Mundsperger, P. J. M. Brouwer, M. Tolazzi, A. Farsang, D. Katinger, J. P. Moore, G. Scarlatti, R. J. Shattock, Q. J. Sattentau and R. W. Sanders, *NPJ Vaccines*, 2021, **6**, 103.

35. M. Neumeier, L. Hails, S. Davis, S. Mann and M. Epple, *J. Mater. Chem.*, 2011, **21**.

36. M. Z. Syeda, T. Hong, C. Huang, W. Huang and Q. Mu, *Cell Death Discov*, 2024, **10**, 117.

37. G. T. Kozma, T. Shimizu, T. Ishida and J. Szebeni, *Adv Drug Deliv Rev*, 2020, **154-155**, 163-175.

38. U. Wattendorf and H. P. Merkle, *J Pharm Sci*, 2008, **97**, 4655-4669.

39. L. Vannucci, E. Falvo, M. Fornara, P. Di Micco, O. Benada, J. Krizan, J. Svoboda, K. Hulikova-Capkova, V. Morea, A. Boffi and P. Ceci, *Int J Nanomedicine*, 2012, **7**, 1489-1509.

40. C. R. O'Riordan, A. Lachapelle, C. Delgado, V. Parkes, S. C. Wadsworth, A. E. Smith and G. E. Francis, *Hum Gene Ther*, 1999, **10**, 1349-1358.

41. Y. Ju, J. M. Carreno, V. Simon, K. Dawson, F. Krammer and S. J. Kent, *Nat Rev Immunol*, 2023, **23**, 135-136.

42. E. J. Yang and I. H. Choi, *Immune Netw*, 2013, **13**, 94-101.

43. J. W. Grunberger, M. A. Dobrovolskaia and H. Ghandehari, *Nanotoxicology*, 2024, **18**, 542-564.

44. M. Kersting, M. Olejnik, N. Rosenkranz, K. Loza, M. Breisch, A. Rostek, G. Westphal, J. Bunger, N. Ziegler, A. Ludwig, M. Koller, C. Sengstock and M. Epple, *Sci Rep*, 2020, **10**, 21591.

45. H. Mouquet, L. Scharf, Z. Euler, Y. Liu, C. Eden, J. F. Scheid, A. Halper-Stromberg, P. N. Gnanapragasam, D. I. Spencer, M. S. Seaman, H. Schuitemaker, T. Feizi, M. C. Nussenzweig and P. J. Bjorkman, *Proc Natl Acad Sci U S A*, 2012, **109**, E3268-3277.

46. S. Bale, G. Goebrecht, A. Stano, R. Wilson, T. Ota, K. Tran, J. Ingale, M. B. Zwick and R. T. Wyatt, *J Virol*, 2017, **91**.

View Article Online
DOI: 10.1039/D5BM01792K

47. A. Almatroudi, *Pharmaceutics*, 2025, **17**.

48. F. Benko, K. Kristo and T. Sovany, *Pharmaceuticals (Basel)*, 2025, **18**.

49. D. Peterhoff, S. Thalhauser, J. M. Sobczak, M. O. Mohsen, C. Voigt, N. Seifert, P. Neckermann, A. Hauser, S. Ding, Q. Sattentau, M. F. Bachmann, M. Breunig and R. Wagner, *Vaccines (Basel)*, 2021, **9**.

50. S. M. Russell and F. Y. Liew, *Nature*, 1979, **280**, 147-148.

51. V. Temchura and K. Uberla, *Curr Opin HIV AIDS*, 2017, **12**, 272-277.

52. D. Damm, E. Suleiman, J. T. Wagner, S. Klessing, F. Pfister, H. Elsayed, B. Walkenfort, J. Stobrawe, J. Mayer, E. Lehner, S. M. Muller-Schmucker, M. Hasenberg, R. T. Wyatt, K. Vorauer-Uhl, V. Temchura and K. Uberla, *Eur J Pharm Biopharm*, 2023, **192**, 112-125.

53. D. Damm, L. Rojas-Sanchez, H. Theobald, V. Sokolova, R. T. Wyatt, K. Uberla, M. Epple and V. Temchura, *Nanomaterials (Basel)*, 2019, **9**.

54. V. Temchura, J. T. Wagner and D. Damm, *Pharmaceutics*, 2023, **16**.

55. S. Thalhauser, D. Peterhoff, R. Wagner and M. Breunig, *J Pharm Sci*, 2020, **109**, 911-921.

View Article Online
DOI: 10.1039/D5BM01792K

Yu Wang *et. al*, Silica-coated papillomavirus-based nanoparticles: a shielded scaffold for HIV-1 vaccines

Data Availability Statement

The data that support the findings of this study are available from the corresponding author upon reasonable request.